Bicyclic Topology Transforms Self-Assembled Nanostructures in Block Copolymer Thin Films

Brian J. Ree[1], *Yusuke Satoh*[2], *Takuya Isono*[1] *and Toshifumi Satoh*[1,*]

[1]Faculty of Engineering, Hokkaido University, Sapporo 060-8628, Japan

[2]Graduate School of Chemical Sciences and Engineering, Hokkaido University, Sapporo 060-8628, Japan

*Correspondence to: satoh@eng.hokudai.ac.jp (T.S.)

ABSTRACT: Ongoing efforts in materials science have resulted in linear block copolymer systems that generate nanostructures via the phase-separation of immiscible blocks; however, such systems are limited with regard to their domain miniaturization and lack of orientation control. We overcome these limitations through the bicyclic topological alteration of a block copolymer system. Grazing incidence X-ray scattering analysis of nanoscale polymer films revealed that bicyclic topologies achieve 51.3–72.8% reductions in domain spacing when compared against their linear analogue, which is more effective than the theoretical predictions for conventional cyclic topologies. Moreover, bicyclic topologies achieve unidirectional orientation and a morphological transformation between lamellar and cylindrical domains with a high structural integrity. Considering the near equivalent volume fraction between the blocks, the formation of hexagonally packed cylindrical domains is particularly noteworthy. Bicyclic topological alteration is therefore a powerful strategy for developing advanced nanostructured materials for microelectronics, displays, and membranes.

KEYWORDS: topological block copolymers, phase separated nanostructures, topological alteration, thin film morphology, unidirectional orientation, grazing incidence X-ray scattering.

Linear block copolymers (*l*-BCPs) have gained significant attention from both academia and industry over the past few decades because of their ability to form a variety of nanostructures based on the phase separations between the block chains. As a result, the resulting nanostructures exhibit potential applications in advanced fields, including lithography,[1–8] membranes,[9–11] drug delivery, [12] biomaterials,[13,14] and rheological modifiers.[15] In terms of determining suitable application for *l*-BCPs, the spacing (i.e., size) of the phase-separated domains has been deemed to be the most crucial factor. More specifically, the mean field theory predicts that smaller domain features in the phase-separated nanostructure of a symmetric *l*-BCP, which are based on fully flexible block chains, can be formed by a lower degree of polymerization (N) and a higher interaction parameter (χ) of the block chains; however, the following condition must be satisfied: $\chi N > 10.5$.[16–20] Such a prediction could be achieved by synthetically optimizing the chemistry, volume fraction f_i, χ, and N values of the block chains of *l*-BCP, and optimizing the processes of nanostructure formation, which include thermal and solvent annealing and substrate surface modification.[1–10,21–31] The domain feature of BCP could be further reduced by changing its molecular topology from linear to cyclic, wherein cyclic BCPs (*c*-BCPs) were reported to reveal 5–16% smaller domains in the bulk state[32–36] and 33% smaller domains in the thin film state.[37] Overall, these domain spacing reductions are less than those (30–37%) predicted theoretically.[38–40] In search for other effective approaches that substantially downsize BCP domains, strategies involving other variations of cyclic topology such as bicyclic or tricyclic, have not been investigated experimentally or theoretically as of yet.

In this work, we successfully demonstrate the extensive size reduction, orientation control, and structural transformation of the phase-separated domain feature of BCP through the use of bicyclic topology. Such domain downsizing is achieved through the use of poly(*n*-decyl glycidyl ether-*block*-2-(2-(2-methoxyethoxy)ethoxy)ethyl glycidyl ether) (PDGE-*b*-PTEGGE)-based materials of equivalent molar block fractions (degree of polymerization, *DP*, of each block is around 50) in three different bicyclic topologies and in their linear BCP counterparts that were previously reported,[41] namely: *Bicycle-A*, *Bicycle-B*, *Bicycle-C*, and *l*-BCP (Figure 1, Table S1 in the Supporting Information). These materials have been chosen specifically for their clear difference in the polarity between the side chains of nonpolar PDGE and polar PTEGGE blocks, narrow dispersity of less than 1.06, and the flexibility of polyether backbone, which make these materials well suited for achieving phase-separation and investigating the impact of bicyclic topology upon thin film morphologies.

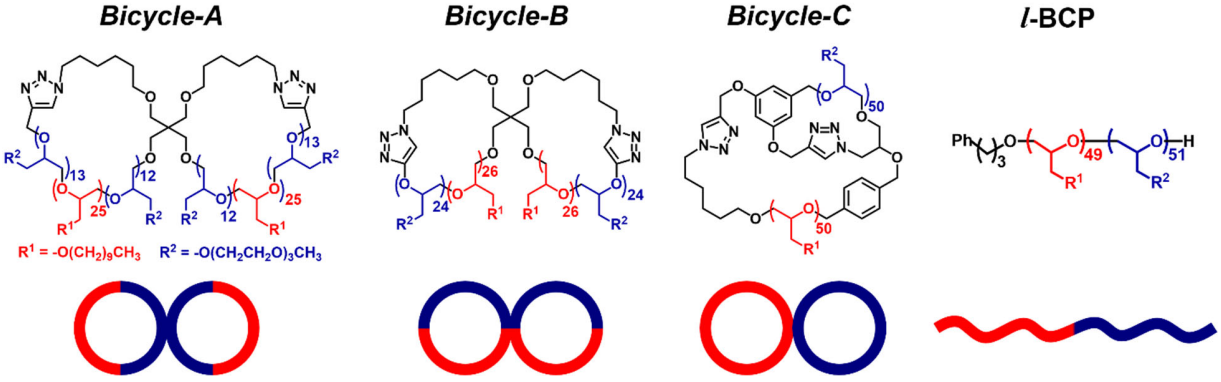

Figure 1. Chemical structures of linear and bicyclic block copolymers investigated in this study: *Bicycle-A* ($M_{n,NMR}$ = 22.2 kDa, M_w/M_n = 1.03, DP_{PDGE} = 50, and DP_{PTEGGE} = 50), *Bicycle-B* ($M_{n,NMR}$ = 21.8 kDa, M_w/M_n = 1.06, DP_{PDGE} = 52, and DP_{PTEGGE} = 48), *Bicycle-C* ($M_{n,NMR}$ = 22.2 kDa, M_w/M_n = 1.04, DP_{PDGE} = 50, and DP_{PTEGGE} = 50), and *l*-BCP ($M_{n,NMR}$ = 21.9 kDa, M_w/M_n = 1.04, DP_{PDGE} = 49, and DP_{PTEGGE} = 51); PDGE blocks are labeled in red, and PTEGGE blocks are labeled in blue. Details of the molecular characteristics are given in Table S1.

All topological polymers of this study reveal glass transitions below -47.1 °C and crystal melting points below 24.9 °C (Figure S1 and Table S2). With these results, the thin films each

block copolymer have been prepared through conventional spin-coating onto silicon substrates with a polymer solution with 0.5 wt% concentration in tetrahydrofuran and filtrated via a disposable syringe equipped with polytetrafluoroethylene filter membrane (0.2 μm pores). After drying in vacuum at room temperature for 24 h, the thicknesses of the polymer films have been measured to range from 100 to 120 nm. The individual film samples have been stored in a vacuum at room temperature prior to grazing incidence small and wide angle X-ray scattering (GISAXS, GIWAXS) measurements, which were also conducted in room temperature. Due to the phase transitions occurring below 24.9 °C, the prepared polymer films are considered to have gained thermal annealing effect through both the drying process and storing period at room temperature.

GIWAXS measurements of the individual films (Figure S2) reveal a weak scattering halo at the scattering angle range of 2 to 4°, which originates from the mean interdistance of the copolymer backbones in random orientation, and a broad scattering halo at the angle range between 12 and 15° that arises from the mean interdistance between the side chains as well as between the side chains and the copolymer backbones. Overall, the GIWAXS analysis confirms that all topological polymer films prepared in this study are amorphous.

Bicycle-A was found to form only a horizontal lamellar nanostructure in the thin films (ca. 100 nm thick) when cast onto bare silicon substrates. The formation of such horizontal lamellar structures was clearly confirmed in the two-dimensional (2D) GISAXS image and quantitative data analysis, as shown in Figure 2. The lamellar structure reveals a domain spacing of 6.93 nm (= D_L, long period) in which each lamella consists of a PTEGGE sublayer 1 (l_1 = 2.35 nm), two interfacial layers (l_2 = 1.10 nm (= l_i)), and a PDGE sublayer (l_3 = 2.38 nm) (Figure 3A; Table S3). The positional distortion factor g is reasonably small (0.12), indicating that a stable lamellar structure was formed in the film. The second order orientation factor O_s is 0.972, which is close to unity, thereby confirming that the lamellar structure is preferentially oriented parallel to the silicon substrate.

These structural characteristics are quite remarkable when compared against the thin film morphological features of *l*-BCP (Table S3; Figure S3). More specifically, the domain spacing is reduced 71.1–72.8% compared to the lamellar domain spacing in the *l*-BCP thin film, which is 1.9–2.4 times greater than those theoretically predicted for cyclic BCPs.[38-40] In addition, the observed *g*-factor is approximately one third that of *l*-BCP, indicating that *Bicycle-A* forms a well-defined lamellar structure with a higher structural integrity than *l*-BCP. Moreover, the horizontal lamella formed by *Bicycle-A* exhibits a unidirectional orientation, which is significantly different from the lamellar structure of its *l*-BCP counterpart, which exhibits a mixture of horizontal and vertical orientations.

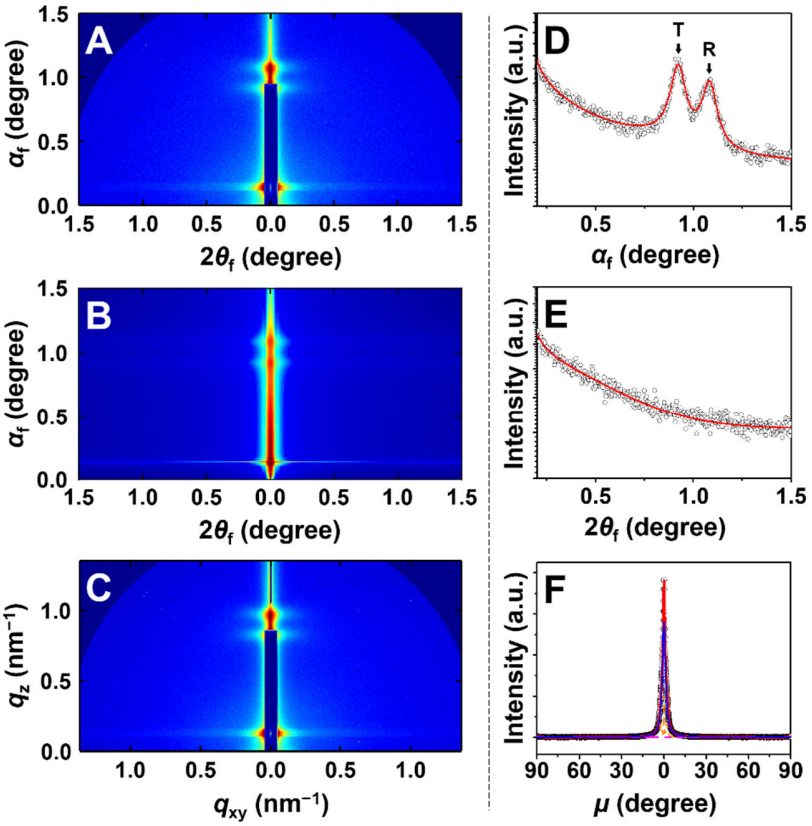

Figure 2. *Bicycle-A*: A lamellar structure with a significantly reduced domain spacing formed in the thin film. (A) 2D GISAXS image in a scattering angle space of the *Bicycle-A* film (ca. 100 nm thick), which was measured with an grazing incidence angle α_i of 0.1447° and a sample-to-detector distance (SDD) of 2909.8 mm at room temperature

using a synchrotron X-ray beam (wavelength $\lambda = 0.12095$ nm); here, α_f and $2\theta_f$ are the out-of-plane and in-plane exit angles of the out-going X-ray beam respectively. (B) 2D GISAXS image reconstructed with the structural parameters determined from quantitative analysis of the image shown in (A). (C) 2D GISAXS image in a scattering vector q space (q_z and q_{xy}) obtained from the image shown in (A). (D) Out-of-plane scattering profile extracted along the meridian line at $2\theta_f = 0.132°$ from the scattering image in (A). (E) In-plane scattering profile along the equatorial line at $\alpha_f = 0.190°$ from the scattering image in (A). In (D, E), the symbols are the measured data, and the solid red lines were obtained by fitting the data using the GIXS formula of the lamellar structure model (details in Supporting Information); the scattering peak generated by the transmitted X-ray beam, is marked "T," whereas that generated by the reflected X-ray beam is marked "R." (F) Azimuthal scattering profile with azimuthal angle μ extracted at $q = 0.833$ nm^{-1} from the scattering image shown in (C) where the black symbols are the measured data and the lines were obtained by deconvolution of the measured data: the blue solid line is the first order scattering peak of the lamellar structure, the purple dotted line is the Yoneda peak, the brown dotted line is part of the reflected X-ray beam, and the red solid line is the sum of all deconvoluted peaks.

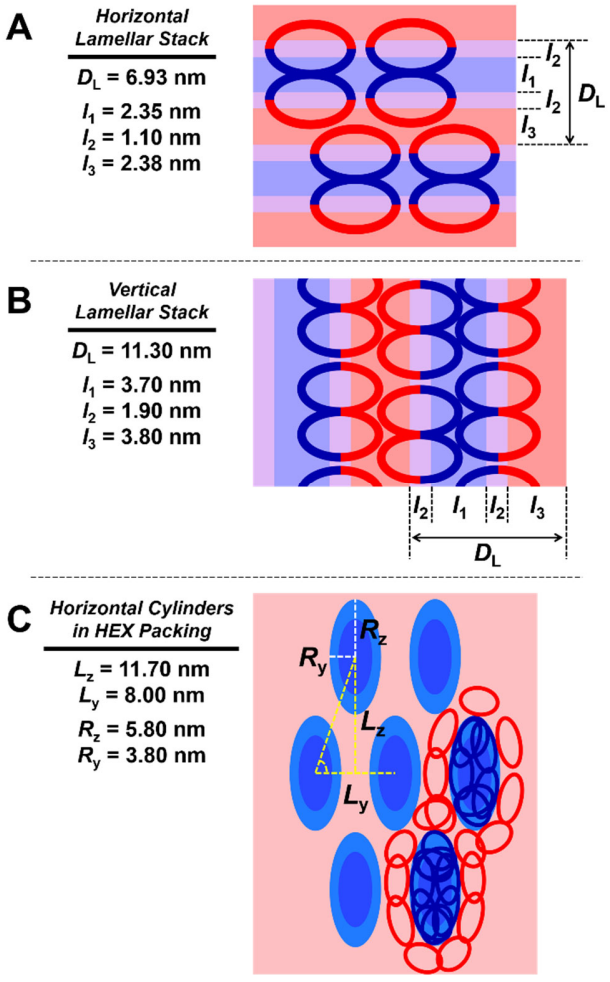

Figure 3. Schematic representations of: (A) lamellar structure (front view) formed in *Bicycle-A* film; considering the volume fractions of the blocks in the copolymer, the l_1 sublayer is assigned as the PTEGGE block phase (blue color), whereas the l_3 sublayer is assigned as the PDGE block phase (red color); (B) lamellar structures (front view) formed in *Bicycle-B* film; considering the volume fractions of the blocks in the copolymer, the l_1 sublayer is assigned as the PTEGGE block phase (blue color), whereas the l_3 sublayer is assigned as the PDGE block phase (red color); (C)

horizontal HEX cylindrical structure (front view) formed in *Bicycle-C* film; the cylinder phase (blue color) is assigned as the PTEGGE block component from the volume fraction (43.4%) of the cylindrical domains obtained from the structural parameters and the volume fractions of the blocks.

Interestingly, *Bicycle-B* also forms a lamellar structure, but the preferred structural orientation is vertical rather than horizontal. This stark contrast to *Bicycle-A* is an astounding result considering that the thin film of *Bicycle-B* has been cast onto the identical bare silicon substrate used for *Bicycle-A* without any surface modification to the substrate (Figures 3B and 4; Table S3). In this case, the domain spacing is 11.30 nm (= D_L), and each lamella is composed of a PTEGGE sublayer 1 (l_1 = 3.70 nm), two interfacial layers (l_2 = 1.90 nm (= l_i)), and a PDGE sublayer (l_3 = 3.80 nm). This domain size is larger than that of *Bicycle-A*, but it has been reduced by 52.9–55.7% from the lamellar domain spacing of *l*-BCP. The overall domain spacing reduction, despite being less than that of *Bicycle-A*, is still greater than those theoretically predicted for cyclic BCPs.

Remarkably, *Bicycle-C* self-assembles into hexagonally (HEX)-packed cylindrical domains rather than lamellar domains (Figures 3C and 5; Table S3). The HEX domain spacing is downsized 51.3–68.6% when compared to that of *l*-BCP, and the magnitude of the domain spacing reduction is 1.4–2.3 times greater than those theoretically predicted for cyclic BCPs. In terms of the structural characteristics of these cylindrical domains, the domain spacing is 11.70 nm (= L_z) along the out-of-plane direction of the film and 8.00 nm (= L_y) along the in-plane direction of the film. The ratio γ of L_z to L_y is 1.46, which is significantly larger than that (= $\sqrt{3}/2$) of a regular HEX structure, consequently indicating that the HEX cylindrical structure is highly distorted along the out-of-plane direction of the film. Such structural distortion is attributed to the highly ellipsoidal nature (ε = 2.23, ellipsoidicity ratio) of the PTEGGE cylindrical domains that present a large radius R_z of 5.80 nm along the out-of-plane direction of the film and a small radius R_y of 2.60 nm along the in-plane direction. Here, the ellipsoidal cylinder consists of two phases, the core and the shell, and

the radii, R_z and R_y, are the sum of the core radius (r_{cz} and r_{cy}) and the shell thickness (t_{sz} and t_{sy}) in their respective directions. The HEX cylindrical structure was confirmed to be both stable (*g*-factor: 0.09) and horizontally well-oriented (orientation factor O_s: 0.980).

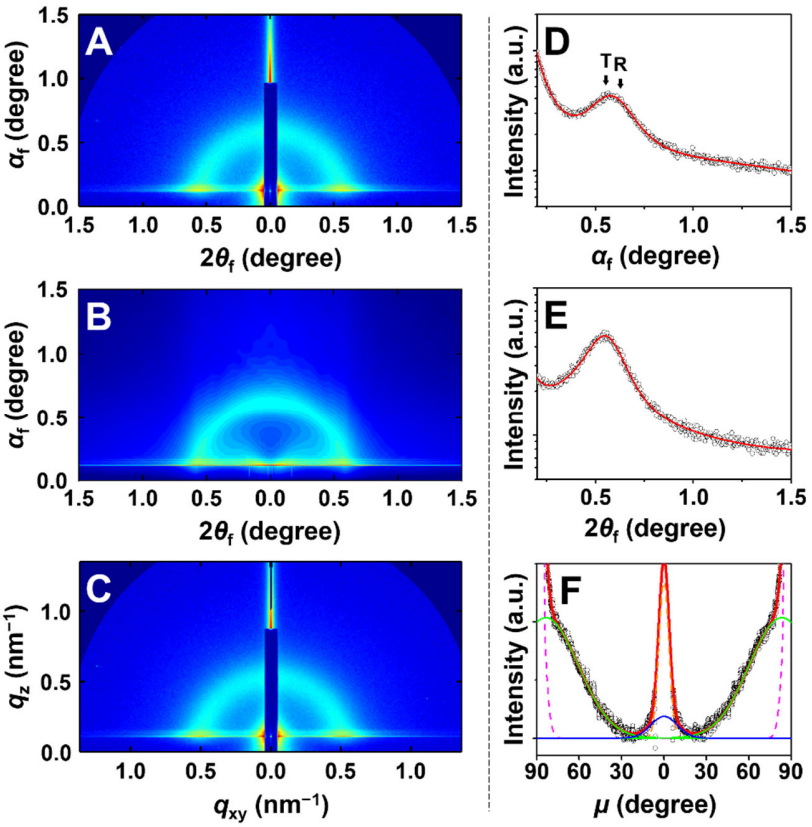

Figure 4. *Bicycle-B*: A lamellar structure with a significantly reduced domain spacing formed in the thin film. (A) 2D GISAXS image in a scattering angle space of the *Bicycle-B* film (ca. 100 nm thick), which was measured with α_i = 0.1283° and SDD = 2909.8 mm at room temperature using a synchrotron X-ray beam (λ = 0.12095 nm). (B) 2D GISAXS image reconstructed with the structural parameters determined from quantitative analysis of the image shown in (A). (C) 2D GISAXS image in a scattering vector q space obtained from the image shown in (A). (D) Out-of-plane scattering profile extracted along the meridian line at $2\theta_f$ = 0.065° from the scattering image shown in (A). (E) In-plane scattering profile along the equatorial line at α_f = 0.201° from the scattering image shown in (A). In (D, E), the symbols are the measured data, and the solid red lines were obtained by fitting the data using the GIXS formula of the lamellar structure model; the scattering peak generated by the transmitted X-ray beam, is marked "T," whereas that generated by the reflected X-ray beam is marked "R." (F) Azimuthal scattering profile with azimuthal angle μ extracted at q = 0.525 nm^{-1} from the scattering image in (C) where the black symbols are the measured data, and the lines were obtained by deconvolution of the measured data: the blue solid line is the first order scattering peak of the horizontal lamellar structure, the green solid line is the first order scattering peak of the vertical lamellar structure, the purple dotted line is the Yoneda peak, the brown dotted line is a part of the reflected X-ray beam, and the red solid line is the sum of all deconvoluted peaks.

As discussed above, the topological alteration of linear PDGE-*b*-PTEGGE into three different *bicyclic* topologies resulted in unique domain features with greatly downsized dimensions that were neither achieved with *l*-BCPs nor predicted theoretically thus far. The three specific forms of the topological alterations, namely *Bicycles-A, -B,* and *-C,* enabled the formation of horizontal lamellar domains, vertical lamellar domains, and horizontal cylindrical domains, respectively, and simultaneously achieved exceptionally small domain sizes. Moreover, the results presented herein provide additional insights into the effects and roles of bicyclic topologies. More specifically, *Bicycle-A* and *Bicycle-B* form lamellar structures, a phenomena aligning with the predictions based on the mean field theory, in addition to the consideration of approximately equivalent volume fractions as well as flexibilities for the PDGE and PTEGGE blocks. The formation of such lamellar structures is further supported by the unique block configurations within their molecular topologies. Both bicyclic topologies can be interpreted to be a pair of smaller cyclic diblock copolymers conjoined at different points. Such cyclic compositions may lead to no discernible or very small amplifications in differentiating one block from another in chain characteristics, thereby causing no substantial shifts in the phase-diagram. As a result, the volume fraction rules apply to both *Bicycle-A* and *Bicycle-B* for the formation of lamellar morphologies. Between *Bicycle-A* and *Bicycle-B*, however, the molecular topology of *Bicycle-A* is more suitable for enhancing the selectivity of each block component on a given substrate surface than *Bicycle-B*, ultimately leading to a horizontally-oriented lamellar structure. In contrast, the molecular topology of *Bicycle-B* plays a key role in anchoring both the PDGE and PTEGGE phases equally onto a given substrate surface, resulting in a vertically-oriented lamellar structure. Finally, the molecular topology of *Bicycle-C* surprisingly forms a HEX cylindrical structure, which is does not obey the volume fraction rule. This result is supported by the fact that the phase-diagram is shifted to the PTEGGE side by a

certain degree through the topological alteration. More specifically, the difference in the block chain characteristics is amplified sufficiently to override the volume fraction rule by cyclization of the PDGE and PTEGGE blocks, thereby shifting the phase diagram and consequently leading to cylindrical PTEGGE domains surrounded by a PDGE matrix.

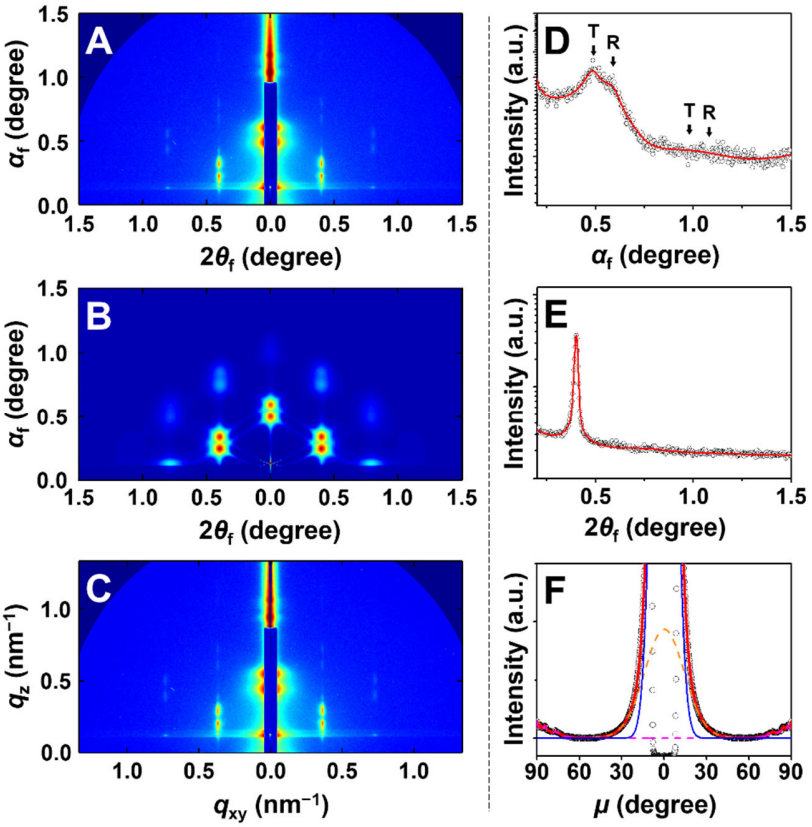

Figure 5. *Bicycle-C*: A cylindrical structure with a significantly reduced domain spacing formed in the thin film. (A) 2D GISAXS image in a scattering angle space of the *Bicycle-C* film (ca. 100 nm thick), which gave values of α_i = 0.1361° and SDD = 2909.8 mm at room temperature using a synchrotron X-ray beam (λ = 0.12095 nm). (B) 2D GISAXS image reconstructed with the structural parameters determined from quantitative analysis of the image shown in (A). (C) 2D GISAXS image in a scattering vector q space obtained from the image shown in (A). (D) Out-of-plane scattering profile extracted along the meridian line at $2\theta_f$ = 0.179° from the scattering image shown in (A): The symbols are the measured data, and the solid red lines were obtained by fitting the data using the GIXS formula of the HEX cylindrical structure model; the scattering peak generated by the transmitted X-ray beam, is marked "T," whereas that generated by the reflected X-ray beam is marked "R." (E) In-plane scattering profile along the equatorial line at α_f = 0.220° from the scattering image shown in (A). (F) Azimuthal scattering profile with azimuthal angle μ extracted at q = 0.450 nm^{-1} from the scattering image shown in (C) where the black symbols are the measured data and the lines were obtained by the deconvolutions of the measured data: The blue and green solid lines are the scattering peaks of the cylindrical domains in the HEX packing order, the purple dotted line is the Yoneda peak, the brown dotted line is a part of the reflected X-ray beam, and the red solid line is the sum of all deconvoluted peaks.

In conclusion, we report three examples of bicyclic topological alteration of *l*-BCP (PDGE-*b*-PTEGGE with equivalent molar block fractions achieving highly downsized phase-separated domains with well-controlled unidirectional orientations. The bicyclic block copolymers, namely *Bicycles-A, -B,* and *-C,* reveal horizontal lamellar (D_L = 6.93 nm), vertical lamellar (D_L = 11.30 nm), and horizontal hexagonally packed cylindrical domains (L_z = 11.70 nm, L_y = 8.00 nm), respectively. In comparison to their linear analogue with same molecular weight, *l*-BCP, revealing a lamellar structure with D_L of 24.00~25.50 nm, the bicyclic block copolymers have achieved minimum domain spacing reduction of 51.3 %, and maximum reduction of 72.8 %. Whereas *Bicycle-A* and *Bicycle-B* form lamellar structures as expected by the volume fraction rule, *Bicycle-C* surprisingly deviates from the rule to form hexagonally packed cylindrical structure with a considerable dimensional distortion that compensates for the equivalent volume fractions of the cylinder and the surrounding matrix. These results demonstrate that, in conjunction with block configuration, bicyclic topological alteration is highly effective in downsizing the domain spacing, increasing the structural integrity, establishing unidirectional orientation, and shifting the phase-diagram of block copolymers. This is a remarkable result showing the potential utilization of bicyclic topological alteration in the context of block copolymer self-assembly applications for developing advanced high-performance materials in various technological fields, such as semiconductors, microelectronics, displays, and membranes.

ASSOCIATED CONTENT

Supporting Information. The Supporting Information is available free of charge at…

Materials, methods, grazing incidence X-ray scattering data analysis, Figure S1, Figure S2, Figure S3, Table S1, Table S2, and Table S3.

AUTHOR INFORMATION

Corresponding Author

Toshifumi Satoh – *Faculty of Engineering, Hokkaido University, Sapporo 060-8628, Japan*; Email: satoh@eng.hokudai.ac.jp

Author Contributions

T.S. supervised the project. B.J.R., Y.S., and T.I. designed the experiments, solved the technical issues, and checked the experimental results. All authors contributed to developing the concept, interpreting the results, and preparing the manuscript.

Funding Sources

This study was supported by a JSPS Grant-in-Aid for Scientific Research (B) (16H04152 and 19H02769 for T.S.), and a MEXT Grant-in-Aid for Scientific Research on Innovative Areas “Hybrid Catalysis” (18H04639 and 20H04789 for T.S.), a JSPS Grant-in-Aid for Challenging Exploratory Research (16K14000 and 19K22209 for T.S.), and a JST CREST (JPMJCR19T4 for T.S.).

Notes

The authors declare no competing interests.

ACKNOWLEDGMENTS

The authors thank the Pohang Accelerator Laboratory for providing opportunities to conduct synchrotron X-ray scattering measurements.

REFERENCES

(1) Tang, C.; Lennon, E. M.; Fredrickson, G. H.; Kramer, E. J.; Hawker, C. J. Evolution of Block Copolymer Lithography to Highly Ordered Square Arrays. *Science* **2008**, *332*, 429–432.

(2) Park, S.; Lee, D. H.; Xu, J.; Kim, B.; Hong, S. W.; Jeong, U.; Xu, T.; Russell, T. P. Macroscopic 10-Terabit–per–Square-Inch Arrays from Block Copolymers with Lateral Order. *Science* **2009**, *323*, 1030-1033.

(3) Kim, H.-C.; Park, S.-M.; Hinsberg, W. D. Block Copolymer Based Nanostructures: Materials, Processes, and Applications to Electronics. *Chem. Rev.* **2010**, *110*, 146–177.

(4) Morris, M. A. Directed Self-assembly of Block Copolymers for Nanocircuitry Fabrication. *Microelectronic Eng.* **2015**, *132*, 207–217.

(5) Nakatani, R.; Takano, H.; Chandra, A.; Yoshimura, Y.; Wang, L.; Suzuki, Y.; Tanaka, Y.; Maeda, R.; Kihara, N.; Minegishi, S.; Miyagi, K.; et al. Perpendicular Orientation Control without Interfacial Treatment of RAFT-Synthesized High-χ Block Copolymer Thin Films with Sub-10 nm Features Prepared via Thermal Annealing. *ACS Appl. Mater. Interfaces* **2017**, *9*, 31266−31278.

(6) Azuma, K.; Sun, J.; Choo, Y.; Rokhlenko, Y.; Dwyer, J. H.; Schweitzer, B.; Hayakawa, T.; Osuji, C. O.; Gopalan, P. Self-Assembly of an Ultrahigh-χ Block Copolymer with Versatile Etch Selectivity. *Macromolecules* **2018**, *51*, 6460−6467.

(7) Luo, Y.; Montarnal, D.; Kim, S.; Shi, W.; Barteau, K. P.; Pester, C. W.; Hustad, P. D.; Christianson, M. D.; Fredrickson, G. H.; Kramer, E. J.; Hawker, C. J. Poly(dimethylsiloxane-b-methyl methacrylate): A Promising Candidate for Sub-10 nm Patterning. *Macromolecules* **2015**, *48*, 3422−3430.

(8) Yoshida, K.; Tanaka, S.; Yamamoto, T.; Tajima, K.; Borsali, R.; Isono, T.; Satoh, T. Chain-End Functionalization with a Saccharide for 10 nm Microphase Separation: “Classical” PS-*b*-PMMA versus PS-*b*-PMMA-Saccharide. *Macromolecules* **2018**, *51*, 8870−8877.

(9) Zalusky, A. S.; Olayo-Valles, R.; Wolf, J. H.; Hillmyer, M. A. Ordered Nanoporous Polymers from Polystyrene−Polylactide Block Copolymers. *J. Am. Chem. Soc.* **2002**, *124*, 12761−12773.
(10) Yoon, J.; Yang, S. Y.; Heo, K.; Lee, B.; Joo, W.; Kim, J. K.; Ree, M. Nondestructive, Quantitative Synchrotron Grazing Incidence X-ray Scattering Analysis of Cylindrical Nanostructures in Supported Thin Films. *J. Appl. Crystallogr.* **2007**, *40*, 305-312.
(11) Yoo, S.; Kim, J.-H.; Shin, M.; Park, H.; Kim, J.-H.; Lee, S.-Y.; Park, S. Hierarchical Multiscale Hyperporous Block Copolymer Membranes via Tunable Dual-Phase Separation, *Science* **2010**, *330*, 349–353.
(12) Liu, R.; Wang, S.; Yao, J.; Xu, W.; Li, H. Cross-Linked Reverse Micelles with Embedded Water Pools: A Novel Catalytic System Based on Amphiphilic Block Copolymers. *RSC Adv.* **2008**, *4*, 38234−38240.
(13) Blanazs, A.; Armes, S. P.; Ryan, A. J. Self−Assembled Block Copolymer Aggregates: From Micelles to Vesicles and their Biological Applications. *Macromol. Rapid Commun.* **2009**, *30*, 267−277.
(14) Ree, B. J.; Satoh, Y.; Jin, K. S.; Isono, T.; Kim, W. J.; Kakuchi, T.; Satoh, T.; Ree, M. Well-Defined and Stable Nanomicelles Self-Assembled from Brush Cyclic and Tadpole Copolymer Amphiphiles: A Versatile Smart Carrier Platform. *NPG Asia Mater.* **2017**, *9*, e453.
(15) Bhatia, S. R.; Mourchid, A.; Joanicot, M. Block Copolymer Assembly to Control Fluid Rheology. *Curr. Opin. Colloid Interface Sci.* **2001**, *6*, 471−478.
(16) Leibler, L. Theory of Microphase Separation in Block Copolymers. *Macromolecules* **1980**, *13*, 1602−1617.
(17) Hashimoto, T.; Shibayama, M.; Kawai, H. Domain-Boundary Structure of Styrene-Isoprene Block Copolymer Films Cast from Solution. 4. Molecular-Weight Dependence of Lamellar Microdomains. *Macromolecules* **1980**, *13*, 1237−1247.
(18) Bates, F. S.; Fredrickson, G. H. Block Copolymer Thermodynamics: Theory and Experiment. *Annu. Rev. Phys. Chem.* **1990**, *41*, 525−557.
(19) Semenov, A. N. Theory of Block Copolymer Interfaces in the Strong Segregation Limit. *Macromolecules* **1993**, *26*, 6617−6621.
(20) Matsen, M. W.; Bates, F. S. Unifying Weak- and Strong-Segregation Block Copolymer Theories. *Macromolecules* **1996**, *29*, 1091−1098.
(21) Sinturel, C.; Bates, F. S.; Hillmyer, M. A. High χ−Low N Block Polymers: How Far Can We Go? *ACS Macro Lett.* **2015**, *4*, 1044−1050.
(22) Yoshimura, Y.; Chandra, A.; Nabae, Y.; Hayakawa, T. Chemically Tailored High-χ Block Copolymers for Perpendicular Lamellae via Thermal Annealing. *Soft Matter* **2019**, *15*, 3497−3506.
(23) Kennemur, J. G.; Yao, L.; Bates, F. S.; Hillmyer, M. A. Sub-5 nm Domains in Ordered Poly(cyclohexylethylene)-*block*-poly(methyl methacrylate) Block Polymers for Lithography. *Macromolecules* **2014**, *47*, 1411–1418.

(24) Lane, A. P.; Yang, X.; Maher, M. J.; Blachut, G.; Asano, Y.; Someya, Y.; Mallavarapu, A.; Sirard, S. M.; Ellison, C. J.; Willson, C. G. Directed Self-Assembly and Pattern Transfer of Five Nanometer Block Copolymer Lamellae. *ACS Nano* **2017**, *11*, 7656−7665.
(25) Kwak, J.; Mishra, A. K.; Lee, J.; Lee, K. S.; Choi, C.; Maiti, S.; Kim, M.; Kim, J. K. Fabrication of Sub-3 nm Feature Size Based on Block Copolymer Self-Assembly for Next-Generation Nanolithography. *Macromolecules* **2017**, *50*, 6813–6818.
(26) Jo, S.; Jeon, S.; Jun, T.; Park, C.; Ryu, D. Y. Fluorine-Containing Styrenic Block Copolymers toward High χ and Perpendicular Lamellae in Thin Films. *Macromolecules* **2018**, *51*, 7152–7159.
(27) Li, X.; Li, J.; Wang, C.; Liu, Y.; Deng, H. Fast Self-assembly of Polystyrene-*b*-poly(fluoro methacrylate) into Sub-5 nm Microdomains for Nanopatterning Applications. *J. Mater. Chem. C* **2019**, *7*, 2535–2540.
(28) Wang, C.; Li, X.; Deng, H. Synthesis of a Fluoromethacrylate Hydroxystyrene Block Copolymer Capable of Rapidly Forming Sub-5 nm Domains at Low Temperatures. *ACS Macro Lett.* **2019**, *8*, 368–373.
(29) Yu, D. M.; Smith, D. A.; Kim, H.; Mapas, J. K. D.; Rzayev, J.; Russell, T. P. Morphological Evolution of Poly(solketal methacrylate)-*block*-polystyrene Copolymers in Thin Films. *Macromolecules* **2019**, *52*, 3592–3600.
(30) Yu, D. M.; Smith, D. A.; Kim, H.; Rzayev, J.; Russell, T. P. Two-Step Chemical Transformation of Polystyrene-*block*-poly(solketal acrylate) Copolymers for Increasing χ. *Macromolecules* **2019**, *52*, 6458–6466.
(31) Wang, H. S.; Oh, S.; Choi, J.; Jang, W.; Kim, K. H.; Arellano, C. L.; Huh, J.; Bang, J.; Im, S. G. High-Fidelity, Sub-5 nm Patterns from High-χ Block Copolymer Films with Vapor-Deposited Ultrathin, Cross-Linked Surface-Modification Layers. *Macromol. Rapid Commun.* **2020**, *41*, 1900514.
(32) Honda, S.; Koga, M.; Tokita, M.; Yamamoto, T.; Tezuka, Y. Phase Separation and Self-Assembly of Cyclic Amphiphilic Block Copolymers with A Main-Chain Liquid Crystalline Segment. *Polym. Chem*. **2015**, *6*, 4167–4176.
(33) Zhu, Y. Q.; Gido, S. P.; Iatrou, H.; Hadjichristidis, N.; Mays, J. W. Microphase Separation of Cyclic Block Copolymers of Styrene and Butadiene and of Their Corresponding Linear Triblock Copolymers. *Macromolecules* **2003**, *36*, 148−152.
(34) Takano, A.; Kadoi, O.; Hirahara, K.; Kawahara, S.; Isono, Y.; Suzuki, J.; Matsushita, Y. Preparation and Morphology of Ring-Shaped Polystyrene-block-polyisoprenes. *Macromolecules* **2003**, *36*, 3045−3050.
(35) Lescanec, R. L.; Hajduk, D. A.; Kim, G. Y.; Gan, Y.; Yin, R.; Gruner, S. M.; Hogen-Esch, T. E.; Thomas, E. L. Comparison of the Lamellar Morphology of Microphase-Separated Cyclic Block Copolymers and Their Linear Precursors. *Macromolecules* **1995**, *28*, 3485−3489.
(36) Lecommandoux, S.; Borsali, R.; Schappacher, M.; Deffieux, A.; Narayanan, T.; Rochas, C. Microphase Separation of Linear and Cyclic Block Copolymers Poly(styrene-*b*-isoprene): SAXS Experiments. *Macromolecules* **2004**, *37*, 1843−1848.

(37) Poelma, J. E.; Ono, K.; Miyajima, D.; Aida, T.; Satoh, K.; Hawker, C. J. Cyclic Block Copolymers for Controlling Feature Sizes in Block Copolymer Lithography. *ACS Nano* **2012**, *6*, 10845−10854.
(38) Marko, J. F. Microphase Separation of Block Copolymer Rings. *Macromolecules* **1993**, *26*, 1442−1444.
(39) Jo, W. H.; Jang, S. S. Monte Carlo Simulation of The Order–Disorder Transition of A Symmetric Cyclic Diblock Copolymer System. *J. Chem. Phys.* **1999**, *111*, 1712−1720.
(40) Zhang, G.; Fan, Z.; Yang, Y.; Qiu, F. Phase Behaviors of Cyclic Diblock Copolymers. *J. Chem. Phys.* **2011**, *135*, 174902.
(41) Isono, T.; Satoh, Y.; Miyachi, K.; Chen, Y.; Sato, S.-i.; Tajima, K.; Satoh, T.; Kakuchi, T. Synthesis of Linear, Cyclic, Figure-Eight-Shaped, and Tadpole Shaped Amphiphilic Block Copolyethers via *t*-Bu-P$_4$-Catalyzed Ring Opening Polymerization of Hydrophilic and Hydrophobic Glycidyl Ethers. *Macromolecules* **2014**, *47*, 2853−2863.

Graphical Table of Contents

Bicyclic Topology Transforms Self-Assembled Nanostructures in Block Copolymer Thin Films

Brian J. Ree, Yusuke Satoh, Takuya Isono, Toshifumi Satoh*